

Imaging tissues and cells beyond the diffraction limit with structured illumination microscopy and Bayesian image reconstruction --Manuscript Draft--

Manuscript Number:	GIGA-D-18-00276R1	
Full Title:	Imaging tissues and cells beyond the diffraction limit with structured illumination microscopy and Bayesian image reconstruction	
Article Type:	Data Note	
Funding Information:	National Institute of General Medical Sciences (1R15GM128166-01)	Dr Guy Hagen
	National Science Foundation (1727033)	Dr Guy Hagen
	SCIEX (13.183)	Dr Tomáš Lukeš
	České Vysoké Učení Technické v Praze (SGS18/141/OHK3/2T/13)	Mr Jakub Pospíšil
	BioFrontiers Institute, University of Colorado Colorado Springs	Dr Guy Hagen
Abstract:	<p>Background</p> <p>Structured illumination microscopy (SIM) is a family of methods in optical fluorescence microscopy that can achieve both optical sectioning and super-resolution effects. SIM is a valuable method for high resolution imaging of fixed cells or tissues labeled with conventional fluorophores, as well as for imaging the dynamics of live cells expressing fluorescent protein constructs. In SIM, one acquires a set of images with shifting illumination patterns. This set of images is subsequently treated with image analysis algorithms to produce an image with reduced out-of-focus light (optical sectioning) and/or with improved resolution (super-resolution).</p> <p>Findings</p> <p>Five complete, freely available SIM datasets are presented including raw and analyzed data. We report methods for image acquisition and analysis using open source software along with examples of the resulting images when processed with different methods. We processed the data using established optical sectioning SIM and super-resolution SIM methods, and with newer Bayesian restoration approaches which we are developing.</p> <p>Conclusion</p> <p>Various methods for SIM data acquisition and processing are actively being developed, but complete raw data from SIM experiments is not typically published. Publically available, high quality raw data with examples of processed results will aid researchers when developing new methods in SIM. Biologists will also find interest in the high-resolution images of animal tissues and cells we acquired. All of the data was processed with SIMToolbox, an open source and freely available software solution for SIM.</p>	
Corresponding Author:	Guy Hagen UNITED STATES	
Corresponding Author Secondary Information:		
Corresponding Author's Institution:		
Corresponding Author's Secondary Institution:		
First Author:	Jakub Pospíšil	

First Author Secondary Information:	
Order of Authors:	Jakub Pospíšil
	Tomáš Lukeš
	Justin Bendesky
	Karel Fliegel
	Kathrin Spendier
	Guy Hagen
Order of Authors Secondary Information:	
Response to Reviewers:	<p>Dear Editor:</p> <p>We would like to resubmit our manuscript entitled “Imaging tissues and cells beyond the diffraction limit with structured illumination microscopy and Bayesian image reconstruction” for consideration in GigaScience as a data note.</p> <p>We would like to thank the referees for their very positive reviews of the paper. Reviewer 1 had a minor point of concern:</p> <p>“One minor point the authors may want to address is the difference between coherent interference illumination and the incoherent pattern illumination employed in the manuscript. It seems that interference illumination can generate a sin pattern with highest contrast at cutoff frequency while incoherent pattern illumination may suffer from the gradually cutoff of the incoherent OTF.”</p> <p>We thank the reviewer for this comment. The reviewer is correct about this, and we have written some comments and added a new reference in the discussion which should clear up this matter. The modified paragraph now reads:</p> <p>“There are several other advantages to the use incoherent illumination in SIM, including removing the need for a pupil plane mask to block unwanted diffraction orders. Also, incoherent imaging of a microdisplay for pattern formation means that the pattern spatial frequency in the sample plane does not depend on the wavelength of the light which is used. On the other hand, in incoherent illumination SIM such as we used here, the contrast of the illumination pattern decreases with increasing spatial frequency according to the incoherent optical transfer function [53]. In coherent illumination SIM [8,9,11], the coherent optical transfer function applies [53], and so the pattern contrast does not decrease with increasing spatial frequency. This means that coherent illumination SIM can more efficiently mix high resolution information from outside the frequency limit into the detection passband of the microscope, thereby potentially achieving better resolution than what we achieved in this work. We achieved a lateral resolution enhancement factor of ~1.8 (Fig. 2), whereas a factor of 2.0 is expected for coherent illumination SIM.”</p> <p>In addition to this, we have fixed a few typographical errors.</p> <p>We hope that the paper will now be acceptable for publication.</p> <p>Sincerely,</p> <p>Guy M. Hagen</p>
Additional Information:	
Question	Response
Are you submitting this manuscript to a special series or article collection?	No
Experimental design and statistics	Yes

<p>Full details of the experimental design and statistical methods used should be given in the Methods section, as detailed in our Minimum Standards Reporting Checklist. Information essential to interpreting the data presented should be made available in the figure legends.</p> <p>Have you included all the information requested in your manuscript?</p>	
<p>Resources</p> <p>A description of all resources used, including antibodies, cell lines, animals and software tools, with enough information to allow them to be uniquely identified, should be included in the Methods section. Authors are strongly encouraged to cite Research Resource Identifiers (RRIDs) for antibodies, model organisms and tools, where possible.</p> <p>Have you included the information requested as detailed in our Minimum Standards Reporting Checklist?</p>	<p>Yes</p>
<p>Availability of data and materials</p> <p>All datasets and code on which the conclusions of the paper rely must be either included in your submission or deposited in publicly available repositories (where available and ethically appropriate), referencing such data using a unique identifier in the references and in the “Availability of Data and Materials” section of your manuscript.</p> <p>Have you have met the above requirement as detailed in our Minimum Standards Reporting Checklist?</p>	<p>No</p>
<p>If not, please give reasons for any omissions below.</p>	<p>we plan to upload the data to GIGA DB when we are contacted by the Gigascience team</p>

as follow-up to "**Availability of data and materials**

All datasets and code on which the conclusions of the paper rely must be either included in your submission or deposited in [publicly available repositories](#) (where available and ethically appropriate), referencing such data using a unique identifier in the references and in the "Availability of Data and Materials" section of your manuscript.

Have you have met the above requirement as detailed in our [Minimum Standards Reporting Checklist](#)?

"

[Click here to view linked References](#)

1
2
3
4 **1 Imaging tissues and cells beyond the diffraction limit with structured illumination microscopy**
5
6 **2 and Bayesian image reconstruction**

7
8
9 **3 Jakub Pospíšil¹, Tomáš Lukeš^{1,2}, Justin Bendesky³, Karel Fliegel¹, Kathrin Spendier^{3,4}, and**
10
11 **4 Guy M. Hagen^{3*}**

12
13
14 ¹Department of Radioelectronics, Faculty of Electrical Engineering, Czech Technical University in
15
16 Prague, Technická 2, 16627 Prague 6, Czech Republic.

17
18 ²Laboratory of Nanoscale Biology, École Polytechnique Fédérale de Lausanne, CH-1015 Lausanne,
19
20 Switzerland.

21
22 ³UCCS center for the Biofrontiers Institute, University of Colorado at Colorado Springs, 1420 Austin
23
24 Bluffs Parkway, Colorado Springs, Colorado, 80918, USA.

25
26
27 ⁴Department of Physics and Energy Science, University of Colorado at Colorado Springs, 1420 Austin
28
29 Bluffs Parkway, Colorado Springs, Colorado, 80918, USA.

30
31 **13 Contact email addresses**

32
33
34 Jakub Pospíšil, pospij27@fel.cvut.cz, ORCID: 0000-0003-3615-5752

35
36 Tomáš Lukeš lukestom@fel.cvut.cz

37
38 Justin Bendesky jbendesk@uccs.edu

39
40 Karel Fliegel, fliegek@fel.cvut.cz, ORCID: 0000-0001-5737-6736

41
42 Kathrin Spendier, kspendie@uccs.edu

43
44
45 Corresponding author, Guy M. Hagen, ghagen@uccs.edu, ORCID: 0000-0002-4802-9481

46
47 **20 Abstract**

48
49 **21 Background:** Structured illumination microscopy (SIM) is a family of methods in optical fluorescence
50
51 microscopy that can achieve both optical sectioning and super-resolution effects. SIM is a valuable
52
53 method for high-resolution imaging of fixed cells or tissues labeled with conventional fluorophores, as
54
55 well as for imaging the dynamics of live cells expressing fluorescent protein constructs. In SIM, one
56
57 acquires a set of images with shifting illumination patterns. This set of images is subsequently treated
58
59
60
61
62
63
64
65

1
2
3
4 26 with image analysis algorithms to produce an image with reduced out-of-focus light (optical sectioning)
5
6 27 and/or with improved resolution (super-resolution).
7
8

9 28 **Findings:** Five complete, freely available SIM datasets are presented including raw and analyzed data.
10
11 29 We report methods for image acquisition and analysis using open source software along with examples
12
13 30 of the resulting images when processed with different methods. We processed the data using established
14
15 31 optical sectioning SIM and super-resolution SIM methods, and with newer Bayesian restoration
16
17 32 approaches which we are developing.
18

19
20 33 **Conclusion:** Various methods for SIM data acquisition and processing are actively being developed, but
21
22 34 complete raw data from SIM experiments is not typically published. Publically available, high quality
23
24 35 raw data with examples of processed results will aid researchers when developing new methods in SIM.
25
26 36 Biologists will also find interest in the high-resolution images of animal tissues and cells we acquired.
27
28 37 All of the data was processed with SIMToolbox, an open source and freely available software solution
29
30 38 for SIM.
31
32

33 39 **Keywords:** super-resolution microscopy, SIMToolbox, structured illumination microscopy, open-source
34
35 40 software, fluorescence, Bayesian methods, LAMP1, live cell imaging.
36
37

38 41 **Data description**

39 42 **Context**

40 43 Several methods are now available which are able to extend the resolution of fluorescence microscopy
41
42 44 beyond the diffraction limit. These methods include photoactivated localization microscopy [1,2]
43
44 45 (PALM, FPALM), stochastic optical reconstruction microscopy [3,4] (STORM, dSTORM), super-
45
46 46 resolution optical fluctuation imaging [5,6] (SOFI), stimulated emission depletion microscopy [7]
47
48 47 (STED), and structured illumination microscopy [8,9] (SIM).
49
50

51 48 Of these various methods, SIM is usually regarded as the most useful for imaging live cells, and
52
53 49 this method has rapidly gained in popularity. Depending on the optical setup and data processing method
54
55 50 used, SIM can achieve optical sectioning (OS-SIM) [10], an effect which greatly reduces out-of-focus
56
57
58
59
60
61
62
63
64
65

1
2
3
4
5
6
7
8
9
10
11
12
13
14
15
16
17
18
19
20
21
22
23
24
25
26
27
28
29
30
31
32
33
34
35
36
37
38
39
40
41
42
43
44
45
46
47
48
49
50
51
52
53
54
55
56
57
58
59
60
61
62
63
64
65

light similar to laser scanning confocal fluorescence microscopy. SIM can also be used for imaging beyond the diffraction limit in fluorescence microscopy. Super-resolution SIM (SR-SIM) [8,9], in its most common implementation [11], uses laser illumination to create a high frequency interference fringe pattern (close to or at the resolution limit of the microscope) to illuminate the sample. In such an experiment, image information with details beyond the limit of spatial frequencies accepted by the microscope is aliased into the acquired images. By acquiring multiple images with shifting illumination patterns, a high-resolution image can be reconstructed [8,9]. Two-dimensional SR-SIM enables a twofold resolution improvement in the lateral dimension [8,9,12,13]. If a three-dimensional illumination pattern is used, a twofold resolution improvement can also be realized in the axial direction [11,14,15]. SIM is perhaps the most attractive super-resolution method for imaging live cells because it does not require high illumination powers, can work with most dyes and fluorescent proteins, uses efficient widefield (WF) detection, and can achieve high imaging rates. SIM has been demonstrated in several applications, including 2D [12,13], and 3D imaging [14,16].

As interest in super-resolution imaging has increased, several alternative approaches for SIM have been introduced which use various kinds of patterned illumination [17–21]. For example, in multifocal structured illumination microscopy (MSIM) [17], a 2D array of focused laser spots is scanned across a sample, and subsequent image processing is used to achieve an image with improved resolution. Structured illumination methods have also been combined with light sheet excitation, a method ideal for imaging live cells [22–26].

In addition to new illumination schemes, alternative data processing methods have also been introduced [27–33]. For example, Orioux et al. suggested a 2D method for SIM reconstruction based on Bayesian estimation [28], and our group showed that Bayesian reconstruction methods in SIM have several potential advantages and can achieve a performance comparable to traditional SIM methods [29]. To allow 3D imaging, our group subsequently introduced maximum *a posteriori* probability SIM (MAP-SIM [30]), a method based on reconstruction of the SIM data using a Bayesian framework. Image

1
2
3
4 76 restoration approaches are useful when working with low signal levels in SIM [34], and have been
5
6
7 77 recently reviewed [35].
8

9 78 We present complete raw and analyzed SIM data from several different situations in cell biology
10
11 79 studies in which we imaged both live and fixed mammalian cells as well as fixed tissues. We used an
12
13 80 alternative approach for SIM illumination which has been previously described [30,36,37]. Our system
14
15 81 uses either light emitting diode (LED) or laser illumination, and a fast ferroelectric liquid crystal-on-
16
17 82 silicon (FLCOS) microdisplay (also known as a spatial light modulator (SLM)) for SIM pattern
18
19 83 definition. SLMs have seen use in SIM and related applications when high speed imaging and flexibility
20
21 84 in controlling the spatial and temporal properties of the illumination are priorities [12–14,16,25,37–43].
22
23 85 To analyze the data we used OS-SIM, SR-SIM, and MAP-SIM methods. All of the raw and analyzed
24
25 86 data are available on GigaDB, and the analysis software (SIMToolbox) is open-source and freely
26
27 87 available [36].
28
29

30 31 88 **Methods**

32 33 89 *Cell lines and reagents*

34
35 90 All cell lines used were maintained in DMEM supplemented with 10% FCS, 100 U/ml penicillin, 100
36
37 91 U/ml streptomycin, and L-glutamate (Invitrogen) at 37 °C and 100% humidity. Cell lines we used for this
38
39 92 study included U2-OS (human bone sarcoma, RRID:CVCL_0042), A431 (human skin carcinoma,
40
41 93 RRID:CVCL_0037), and Hep-G2 (human liver carcinoma, RRID:CVCL_0027).
42
43

44 45 94 *Preparation of samples for imaging*

46
47 95 (SIM data 1, Fig. 4) U2-OS cells expressing lysosome-associated membrane protein 1 labeled with green
48
49 96 fluorescent protein (LAMP1-GFP) were grown in petri dishes with coverslip bottoms (MatTek) for 24
50
51 97 hours, then imaged them in full medium at room temperature. In this experiment, we used microscopy
52
53 98 system 1 (Olympus IX71, Table 2).
54
55

56 99 (SIM data 2, Fig. 5) A431 cells were grown on #1.5H coverslips (Marienfeld) for 48 hours in
57
58 100 normal medium. We washed the cells once with phosphate buffered saline (PBS), pH 7.4, and then
59
60
61
62
63
64
65

1
2
3
4
5
6
7
8
9
10
11
12
13
14
15
16
17
18
19
20
21
22
23
24
25
26
27
28
29
30
31
32
33
34
35
36
37
38
39
40
41
42
43
44
45
46
47
48
49
50
51
52
53
54
55
56
57
58
59
60
61
62
63
64
65

101 treated the cells with 5 μ M DiI-C₁₆ (Molecular Probes) in PBS at room temperature for 5 minutes. This
102 probe is a lipid modified with a fluorescent dye that inserts into the plasma membrane of live mammalian
103 cells within a few minutes. We then washed the cells twice with PBS, then imaged them on the SIM
104 system in fresh PBS at room temperature using a coverslip chamber (Biotech). In this experiment, we
105 used microscopy system 3 (Leica DMI8, Table 2).

106 (SIM data 3, Fig. 6) A prepared slide was acquired (AmScope) containing sectioned rabbit testis
107 stained with hematoxylin and eosin (H&E). In this experiment, we used microscopy system 3 (Leica
108 DMI8, Table 2).

109 (SIM data 4, Fig. 7) Hep-G2 cells expressing Dendra2-histone 4 [44] were grown on #1.5H
110 coverslips for 24 hours, then fixed for 15 minutes at room temperature with 4% paraformaldehyde. We
111 then permeabilized the cells for 5 minutes at room temperature with 0.1% triton-X100, then washed the
112 cells with PBS. We then labeled the actin cytoskeleton of the cells for 1 hour at room temperature with 5
113 nM Atto 565 phalloidin, followed by washing the cells with PBS. We finally mounted the coverslips on
114 clean slides using mowiol 4-88 (Fluka). In this experiment, we used microscopy system 1 (Olympus
115 IX71, Table 2).

116 (SIM data 5, Fig. 8) A prepared slide was acquired (Molecular Probes) containing bovine
117 pulmonary endothelial (BPAE) cells stained with Alexa Fluor 488 phalloidin (to label the actin
118 cytoskeleton) and Mitotracker CMXRos (to label mitochondria). In this experiment, we used microscopy
119 system 2 (Olympus IX83, Table 2).

120 Table 1 summarizes the imaging parameters used for the different samples.

121 *Microscope setup and acquisition*

122 We used three different home-built SIM setups based on the same general design as described
123 previously [30,36,37] (Figure 1). The three SIM systems were based on Olympus IX71, Olympus IX83,
124 and Leica DMI8 microscopes coupled with sCMOS cameras (Andor) under the control of IQ3 software
125 (Andor). The parameters of the different microscope setups are shown in Table 2.

1
2
3
4
5 126 In each microscope setup, the illumination patterns were produced by a high-speed ferroelectric
6
7 127 liquid crystal on silicon (FLCOS) microdisplay (SXGA-3DM, Forth Dimension Displays, 13.6 μm pixel
8
9 128 pitch). This particular FLCOS microdisplay has been used previously in SIM [14,16,25,29,30,36,37,45–
10
11 129 48], and in other optical sectioning systems such as programmable array microscopy (PAM) [38,42,49].
12
13 130 The display was illuminated by a home-built, three channel LED system based on high power LEDs (PT-
14
15 131 54 or PT-120 with DK-114N or DK-136M controller, Luminous Devices) with emission maxima at
16
17 132 460 nm, 525 nm, and 623 nm. The output of each LED was filtered with a band pass filter (Chroma), and
18
19 133 the three wavelengths were combined with appropriate dichroic mirrors (Chroma). The light was then
20
21 134 vertically polarized with a linear polarizer (Edmund Optics). We imaged the microdisplay into the
22
23 135 microscope using an external tube lens (Table 2) and polarizing beam splitter cube (Thor Labs). With any
24
25 136 of the setups and when using a 100 \times objective, single microdisplay pixels are imaged into the sample
26
27 137 with a nominal size of 136 nm, thus as diffraction-limited spots. This is important for achieving the
28
29 138 highest resolution results [37]. More details are available in the supplementary material of [36]. In one
30
31 139 experiment (Figure 8) we used a Spectra-X light source (Lumencor).

32
33
34
35
36 140 The microdisplay allows one to create any desired illumination pattern. In our experiments, the
37
38 141 illumination masks consisted of line grids of different orientations (0° , 90° , 45° and 135°). The lines were
39
40 142 one microdisplay pixel thick (diffraction limited in the sample when using a 100 \times objective) with a gap
41
42 143 of “off” pixels in between. The illumination line grid was shifted by one pixel between each image
43
44 144 acquisition to obtain a shifted illumination mask. The shift between each image was constant, and the
45
46 145 sum of all illumination masks resulted in homogenous illumination. Our optical setup, in which an
47
48 146 incoherently illuminated microdisplay is imaged into the sample with highly corrected microscope optics,
49
50 147 results in much more stable SIM illumination parameters compared to conventional SIM in which the
51
52 148 illumination pattern is created by laser interference. We use a unique spatial calibration method to
53
54 149 determine, with very high accuracy, the position of the patterned illumination in the sample [37]. This is
55
56
57
58
59
60
61
62
63
64
65

1
2
3
4 150 a spatial domain process and does not rely on fitting of data to a model except for the assumption that the
5
6
7 151 imaging is linear and shift-invariant.
8

9 152 **Insert Figure 1**

10
11 153 **Table 1 Imaging parameters for the SIM datasets**

Data	sample	Label (structure)	Pixel size, nm	Illumination	Exposure time, ms	SIM experiment type	SIM pattern # of angles/phases	Microscope system used
SIM data 1 (Fig. 4)	Live U2-OS cells	LAMP1-GFP (lysosomes and membrane)	65	LED 480 nm	25	2D time lapse	1/11	1
SIM data 2 (Fig. 5)	Live A431 cells	Dil-C16 (membrane)	65	LED 530 nm	100	3D	4/24	3
SIM data 3 (Fig. 6)	Fixed rabbit testis	Hematoxylin and eosin (structural strain)	65	LED 530 nm	200	3D	1/11	3
SIM data 4 (Fig. 7)	Fixed Hep-G2 cells	Dendra2-H4 (nucleus) Atto565-phalloidin (actin)	65	LED 480 nm LED 530 nm	500	3D	4/24	1
SIM data 5 (Fig. 8)	Fixed BPAE cells	AlexaFluor 488 phalloidin (actin) Mitotracker CMXRos (mitochondria)	65	Lumencor spectra-X 470 nm 550 nm	300	2D	1/11	2

14
15
16
17
18
19
20
21
22
23
24
25
26
27
28
29
30
31
32
33
34 154

35
36 155 **Table 2 Parameters of the microscope systems**

Setup	Microscope	Objective	sCMOS Camera	Illumination tube lens focal length and part number
1	Olympus IX71	100x/1.4 UPLSAPO	Andor Neo 5.5	180 mm U-TLU
2	Olympus IX83	100x/1.3 UPLFLN	Andor Zyla 4.2+	180 mm SWTLU-C
3	Leica DMI8	100x/1.47 HCX PLAPO TIRF	Andor Zyla 4.2+	200 mm 11525408

37
38
39
40
41
42
43
44
45
46 156

47
48 157 *Data processing methods*

49
50 158 We processed all of the data presented here using SIMToolbox, an open source, user friendly, and freely
51
52
53 159 available program which our group developed for processing SIM data [36]. SIMToolbox, sample data,
54
55 160 and complete documentation are freely available (<http://mmtg.fel.cvut.cz/SIMToolbox>). SIMToolbox is
56
57 161 capable of OS-SIM [10,37], SR-SIM [8,9], and MAP-SIM [30] methods. See the supplementary
58
59 162 information for additional details about these methods.
60
61
62
63
64
65

1
2
3
4
5
6
7
8
9
10
11
12
13
14
15
16
17
18
19
20
21
22
23
24
25
26
27
28
29
30
31
32
33
34
35
36
37
38
39
40
41
42
43
44
45
46
47
48
49
50
51
52
53
54
55
56
57
58
59
60
61
62
63
64
65

163 *Resolution measurements - spatial domain method*

164 Previously, we used microscopy setup 1 (Olympus IX71) to measure spatial resolution by averaging
165 spatial measurements from fifty individual 100 nm fluorescent beads [30]. We used a 100×/1.40 NA oil
166 immersion objective and 460 nm LED excitation (emission 500 - 550 nm). A 19 × 19 pixel region of
167 interest (ROI) was selected around each bead in both the widefield and MAP-SIM images. The ROIs
168 were then registered with sub-pixel accuracy using normalized cross-correlation. Each ROI was fit with
169 a Gaussian function and the full width at half maximum (FWHM) was determined in the axial and lateral
170 directions. Figure 2 shows the resulting averaged FWHM values and PSF cross-sections [30].

171 **Insert Figure 2**

172 *Resolution measurements - frequency domain method*

173 It is desirable to measure the actual resolution achieved in SIM images (or image sequences) of cells or
174 tissues, but suitable structures are not always present in the images. We therefore developed a robust
175 frequency domain method which can be used to measure resolution in any fluorescence microscopy
176 image [50].

177 The power spectral density (PSD) describes the distribution of the power of a signal with respect
178 to its frequency. The PSD of an image is the squared magnitude of its Fourier transform, and can be
179 written as

$$\text{PSD}(k,l) = |\mathcal{F}\{I(m,n)\}|^2 \quad (1)$$

181 where \mathcal{F} represents the Fourier transform, $I(m,n)$ is the image intensity, m,n indexes the rows and
182 columns of the 2D image, respectively, and (k,l) are coordinates in the frequency domain. In polar
183 coordinates, the circularly averaged PSD (PSD_{ca}) in frequency space with frequency q and angle θ is
184 given as

$$\text{PSD}_{\text{ca}} = 10 \cdot \log_{10} \left(\frac{1}{N_q} \sum_{\theta} \text{PSD}(q,\theta) \right) \quad (2)$$

1
2
3
4
5
6
7
8
9
10
11
12
13
14
15
16
17
18
19
20
21
22
23
24
25
26
27
28
29
30
31
32
33
34
35
36
37
38
39
40
41
42
43
44
45
46
47
48
49
50
51
52
53
54
55
56
57
58
59
60
61
62
63
64
65

186 which averages PSD at spatial frequency q . N_q is the number of pixels at a particular frequency q . The
187 resolution limit in real space corresponds to the cut-off frequency in Fourier space. Assuming a noiseless
188 case, the cut-off frequency will be equal to the spatial frequency at which PSD_{ca} drops to zero. In
189 practice, PSD_{ca} contains non-zero values over the whole frequency range caused by noise. The signal to
190 noise ratio (SNR) in Fourier space is generally very low close to the cut-off frequency, which makes
191 precise detection of the cut-off frequency challenging. For this we use a spectral subtraction method [50].
192 Assuming additive noise, in the frequency domain we can write

$$\tilde{X}(k) = Y(k) - E[N(k)] \tag{3}$$

194 where Y , \tilde{X} , and $E[N(k)]$ represent the noisy signal, the desired signal, and the noise spectrum estimate
195 (expected noise spectrum), respectively. The noise spectrum $|N(k)|$ is estimated from the parts of signal
196 where only noise is present. If the spatial sampling is high enough to fulfill the Nyquist–Shannon
197 criterion and oversamples the resolution limit of the reconstructed SIM image, spatial frequencies close
198 to the half of the sampling frequency do not contain useful signal and can be used for noise estimation.
199 We varied the frequency cut-off threshold over the range $\langle 0.95f_{\text{max}}; f_{\text{max}} \rangle$, estimated the level of noise for
200 every threshold value, and obtained the mean and variance of the cut-off frequency (i.e. the resolution
201 estimate). The f_{max} is given by $f_{\text{max}} = f_s/2 = 1/2p_{xy}$, where f_s and p_{xy} are the sampling frequency and the
202 backprojected pixel size, respectively.

203 Figure 3 shows the PSD_{ca} and corresponding resolution limit measured for the data shown in Fig.
204 5. Using our resolution estimation algorithm, we calculated a lateral spatial resolution of 294 nm for WF,
205 and 141 nm for MAP-SIM. The measured resolution is in approximate agreement with our results
206 measured on 100 nm fluorescent beads (Fig. 2).

207 **Insert Figure 3**

1
2
3
4 208 *Imaging live cells, fixed cells, and tissues with SIM*

5
6
7 209 To demonstrate the utility of our approach in imaging live cells, we imaged U2-OS cells that had been
8
9 210 transfected with GFP-tagged lysosomal associated membrane protein (LAMP1-GFP). LAMP1 is a highly
10
11 211 glycosylated protein which is found on the surface of lysosomes and in the plasma membrane [51]. Fig. 4
12
13 212 shows widefield, OS-SIM, and MAP-SIM images of U2-OS cells expressing LAMP1-GFP, and the fast
14
15 213 Fourier transform (FFT) of each image. The dotted circles in Fig. 4(d-f) show the approximate limit of
16
17 214 resolution in each image. We found that, in addition to lysosomal expression, LAMP1-GFP is also
18
19 215 present in high concentrations in the plasma membrane of U2-OS cells.

20
21
22 216 In this experiment, we acquired SIM image sequences with an exposure time of 25 ms, a raw
23
24 217 imaging rate of 40 Hz. We used a SIM pattern with 11 phases (pattern period in the sample plane 1.5 μm)
25
26 218 and a single angle (0° with respect to the camera), acquiring 3982 total frames, resulting in 472 processed
27
28 219 frames (see table 1). The imaging rate of processed result frames was therefore 3.6 Hz. The full image
29
30 220 sequence is available at http://mmtg.fel.cvut.cz/mapsimlive_suppl/ and also available at GigaDB[52].
31
32 221 We further analyzed this data as shown in the supplementary material (Figure S2-S3).

33
34 222 **Insert Figure 4**

35
36
37
38 223 We next imaged live A431 cells which we labeled with the fluorescent lipid DiI-C16. In this experiment
39
40 224 we acquired SIM image sequences with an exposure time of 100 ms, a raw imaging rate of 10 Hz. We
41
42 225 used a SIM pattern with 24 total phases and four angles (see table 1). This data is shown in Figure 5.

43
44 226 **Insert Figure 5**

45
46
47 227 Figure 6 shows SIM imaging of fixed tissues, in this case the seminiferous tubule of the rabbit stained
48
49 228 with hematoxylin and eosin.

50
51 229 **Insert Figure 6**

52
53 230 Figure 7 shows SIM imaging of fixed HEPG2 cells expressing H4-Dendra, a nuclear marker. We also
54
55 231 stained the cells with Atto 532-phalloidin to label the actin cytoskeleton.

56
57
58 232 **Insert Figure 7**
59
60
61
62
63
64
65

1
2
3
4
5
6
7
8
9
10
11
12
13
14
15
16
17
18
19
20
21
22
23
24
25
26
27
28
29
30
31
32
33
34
35
36
37
38
39
40
41
42
43
44
45
46
47
48
49
50
51
52
53
54
55
56
57
58
59
60
61
62
63
64
65

233 Figure 8 shows SIM imaging of fixed BPAE cells labeled with Alexa 488-phalloidin and mitotracker
234 CMXRos to visualize the actin cytoskeleton and mitochondria, respectively.

235 **Insert Figure 8**

236 **5. Discussion**

237 SIM results sometimes suffer from artifacts related to the illumination pattern. The artifacts, which can
238 be severe and are a cause for concern, can be due to several factors including illumination pattern phase
239 instability and pattern distortion because of refractive index mismatch between the sample and the
240 immersion fluid. In our hands, MAP-SIM results do not suffer from detectable patterned artifacts, Fig.
241 4(c), and the FFT of the MAP-SIM result is free of noticeable spurious peaks, Fig. 4(f). We attribute this
242 to several factors, primarily the use of incoherent illumination together with a FLCOS microdisplay for
243 pattern generation. This, combined with precise synchronization of the SIM system helps eliminate
244 patterned artifacts. Additional artifacts in SIM images can arise due to the detector. In sCMOS cameras
245 like the one we used, each pixel reads out through its own amplifier and as such, each pixel exhibits a
246 different gain. While very minor, such artifacts can be corrected using a variance stabilization method as
247 has been introduced for single molecule localization microscopy [53].

248 There are several other advantages to the use incoherent illumination in SIM, including removing the
249 need for a pupil plane mask to block unwanted diffraction orders. Also, incoherent imaging of a
250 microdisplay for pattern formation means that the pattern spatial frequency in the sample plane does not
251 depend on the wavelength of the light which is used. On the other hand, in incoherent illumination SIM
252 such as we used here, the contrast of the illumination pattern decreases with increasing spatial frequency
253 according to the incoherent optical transfer function [54]. In coherent illumination SIM [8,9,11], the
254 coherent optical transfer function applies [54], and so the pattern contrast does not decrease with
255 increasing spatial frequency. This means that coherent illumination SIM can more efficiently mix high
256 resolution information from outside the frequency limit into the detection passband of the microscope,
257 thereby potentially achieving better resolution than what we achieved in this work. We achieved a lateral

1
2
3
4 258 resolution enhancement factor of ~ 1.8 (Fig. 2), whereas a factor of 2.0 is expected for coherent
5
6 259 illumination SIM.
7
8

9 260 The FLCOS microdisplay (and vendor-supplied microdisplay-timing program) we used can display
10
11 261 an illumination pattern and switch to the next pattern in the sequence in 1.14 ms, allowing unprocessed
12
13 262 SIM images to be acquired at rates of approximately 875 Hz. However, such rapid imaging is not useful
14
15 263 if the reconstructed SIM images are of poor quality, for example if they suffer from low signal to noise
16
17 264 ratios. Specifying the fastest possible acquisition rate is inadequate without consideration of the
18
19 265 resolution and SNR of the results. Our resolution analysis shown in Figs. 2-4 (see also supplementary
20
21 266 figure 4) uses measured quantities to evaluate SIM results and thereby helps to make realistic conclusions
22
23
24 267 about imaging speeds.
25
26

27 268 **6. Re-use potential**

28
29 269 The presented SIM datasets can be reused in several ways. Researchers investigating SIM reconstruction
30
31 270 algorithms can use the datasets to compare their results with those presented here, including the newer
32
33 271 method MAP-SIM. Also, the data may be further analyzed in other ways. One possibility is shown in the
34
35 272 supplementary material (part 2: single particle tracking experiments in LAMP1-GFP cells.) Here, we
36
37 273 used single particle tracking methods to study the mobility of lysosomes within U2-OS cells.
38
39

40 274 **Availability of source code and requirements**

41
42 275 Project name: SIMToolbox v1.3
43

44
45 276 Project home page: <http://mmtg.fel.cvut.cz/SIMToolbox/>
46

47 277 Operating system: platform independent
48

49 278 Programming language: MATLAB
50

51 279 License: GNU General Public License v3.0
52

53 280 **Detailed software compatibility notes**

54
55
56 281 The SIMToolbox GUI was compiled with MATLAB 2015a and tested in Windows 7 and 8. The GUI is a
57
58 282 stand-alone program and does not require MATLAB to be installed. To use the MATLAB functions
59
60
61
62
63
64
65

1
2
3
4
5
6
7
8
9
10
11
12
13
14
15
16
17
18
19
20
21
22
23
24
25
26
27
28
29
30
31
32
33
34
35
36
37
38
39
40
41
42
43
44
45
46
47
48
49
50
51
52
53
54
55
56
57
58
59
60
61
62
63
64
65

283 within SIMToolbox (i.e., without the GUI), MATLAB must be installed. The functions were mainly
284 developed with 64 bit MATLAB versions 2012b, 2014a, 2015a in Windows 7. When using SIMToolbox
285 functions without the GUI, the MATLAB “Image Processing Toolbox” is required. SIMToolbox also
286 requires the “MATLAB YAML” package to convert MATLAB objects to/from YAML file format. Note
287 that this package is installed automatically when using the GUI.

288 **Availability of data**

289 All raw and analyzed data is available in the *GigaScience* GigaDB database [52].

290 **Abbreviations**

291 GFP: green fluorescent protein; GUI: graphical user interface; NA: numerical aperture; PSF: point spread
292 function; PSD: power spectral density; PSDca, circularly averaged power spectral density; SBR: signal to
293 background ratio; SIM: structured illumination microscopy; SNR: signal to noise ratio; WF: wide field.

294 **Ethics approval and consent to participate**

295 Not applicable

296 **Consent for publication**

297 Not applicable

298 **Competing interests**

299 The authors declare that they have no competing interests.

300 **Funding**

301 This work was supported by the National Institutes of Health grant number 1R15GM128166-01. This
302 work was also supported by the UCCS center for the University of Colorado BioFrontiers Institute, by
303 the Czech Science Foundation, and by Czech Technical University in Prague (grant number
304 SGS18/141/OHK3/2T/13). T.L. acknowledges a SCIEX scholarship (project code 13.183). The funding
305 sources had no involvement in study design; in the collection, analysis and interpretation of data; in the
306 writing of the report; or in the decision to submit the article for publication. This material is based in part
307 upon work supported by the National Science Foundation under Grant Number 1727033. Any opinions,

1
2
3
4
5
6
7
8
9
10
11
12
13
14
15
16
17
18
19
20
21
22
23
24
25
26
27
28
29
30
31
32
33
34
35
36
37
38
39
40
41
42
43
44
45
46
47
48
49
50
51
52
53
54
55
56
57
58
59
60
61
62
63
64
65

308 findings, and conclusions or recommendations expressed in this material are those of the authors and do
309 not necessarily reflect the views of the National Science Foundation.

310 **Author Contributions**

311 TL: analyzed data, developed computer code

312 JP: analyzed data, developed computer code

313 KF: supervised research

314 KS: analyzed data

315 JB: acquired data

316 GH: conceived project, acquired data, analyzed data, supervised research, wrote the paper

317 **Acknowledgements**

318 The authors thank Dr. Donna Arndt-Jovin and Dr. Tomas Jovin of the Max Planck Institute for
319 Biophysical Chemistry (Göttingen, Germany) for the A431 cells. The authors thank Viola Hausnerová
320 and Christian Lanctôt of Charles University in Prague (Prague, Czech Republic), for the LAMP1-GFP
321 cells. The authors thank Pavel Křížek, Zdeněk Švindrych, and Martin Ovesný for help with data
322 acquisition, microscopy development, programming, and data analysis.

323 **References**

- 324 1. E. Betzig, G. H. Patterson, R. Sougrat, O. W. Lindwasser, S. Olenych, J. S. Bonifacino, M. W.
325 Davidson, J. Lippincott-Schwartz, and H. F. Hess, "Imaging intracellular fluorescent proteins at
326 nanometer resolution," *Science* **313**, 1642–5 (2006).
- 327 2. S. T. Hess, T. P. K. Girirajan, and M. D. Mason, "Ultra-high resolution imaging by fluorescence
328 photoactivation localization microscopy," *Biophys. J.* **91**, 4258–4272 (2006).
- 329 3. M. J. Rust, M. Bates, and X. Zhuang, "Sub-diffraction-limit imaging by stochastic optical
330 reconstruction microscopy (STORM)," *Nat. Methods* **3**, 793–795 (2006).
- 331 4. M. Heilemann, S. van de Linde, M. Schüttpelz, R. Kasper, B. Seefeldt, A. Mukherjee, P.
332 Tinnefeld, and M. Sauer, "Subdiffraction-resolution fluorescence imaging with conventional

1
2
3
4
5
6
7
8
9
10
11
12
13
14
15
16
17
18
19
20
21
22
23
24
25
26
27
28
29
30
31
32
33
34
35
36
37
38
39
40
41
42
43
44
45
46
47
48
49
50
51
52
53
54
55
56
57
58
59
60
61
62
63
64
65

fluorescent probes," *Angew. Chemie Int. Ed.* **47**, 6172–6176 (2008).

334 5. T. Dertinger, R. Colyer, G. Iyer, S. Weiss, and J. Enderlein, "Fast, background-free, 3D super-
335 resolution optical fluctuation imaging (SOFI)," *Proc. Natl. Acad. Sci. U. S. A.* **106**, 22287–22292
336 (2009).

337 6. S. Geissbuehler, N. L. Bocchio, C. Dellagiacoma, C. Berclaz, M. Leutenegger, and T. Lasser,
338 "Mapping molecular statistics with balanced super-resolution optical fluctuation imaging
339 (bSOFI)," *Opt. Nanoscopy* **1**, 4 (2012).

340 7. S. W. Hell and J. Wichmann, "Breaking the diffraction resolution limit by stimulated emission:
341 stimulated-emission-depletion fluorescence microscopy," *Opt. Lett.* **19**, 780 (1994).

342 8. R. Heintzmann and C. Cremer, "Laterally modulated excitation microscopy: improvement of
343 resolution by using a diffraction grating," *Proc. SPIE* **3568**, 185–196 (1998).

344 9. M. G. L. Gustafsson, "Surpassing the lateral resolution limit by a factor of two using structured
345 illumination microscopy," *J. Microsc.* **198**, 82–87 (2000).

346 10. M. A. A. Neil, R. Juškaitis, and T. Wilson, "Method of obtaining optical sectioning by using
347 structured light in a conventional microscope," *Opt. Lett.* **22**, 1905–1907 (1997).

348 11. M. G. L. Gustafsson, L. Shao, P. M. Carlton, C. J. R. Wang, I. N. Golubovskaya, W. Z. Cande, D.
349 A. Agard, and J. W. Sedat, "Three-dimensional resolution doubling in widefield fluorescence
350 microscopy by structured illumination," *Biophys. J.* **94**, 4957–4970 (2008).

351 12. P. Kner, B. B. Chhun, E. R. Griffis, L. Winoto, and M. G. L. Gustafsson, "Super-resolution video
352 microscopy of live cells by structured illumination," *Nat. Methods* **6**, 339–342 (2009).

353 13. L. M. Hirvonen, K. Wicker, O. Mandula, and R. Heintzmann, "Structured illumination
354 microscopy of a living cell," *Eur. Biophys. J.* **38**, 807–812 (2009).

355 14. L. Shao, P. Kner, E. H. Rego, and M. G. L. Gustafsson, "Super-resolution 3D microscopy of live
356 whole cells using structured illumination," *Nat. Methods* **8**, 1044–1046 (2011).

357 15. L. Schermelleh, P. M. Carlton, S. Haase, L. Shao, L. Winoto, P. Kner, B. Burke, M. C. Cardoso,

1
2
3
4
5
6
7
8
9
10
11
12
13
14
15
16
17
18
19
20
21
22
23
24
25
26
27
28
29
30
31
32
33
34
35
36
37
38
39
40
41
42
43
44
45
46
47
48
49
50
51
52
53
54
55
56
57
58
59
60
61
62
63
64
65

358 D. A. Agard, M. G. L. Gustafsson, H. Leonhardt, and J. W. Sedat, "Subdiffraction multicolor
359 imaging of the nuclear periphery with 3D structured illumination microscopy," *Science* **320**,
360 1332–1336 (2008).

361 16. R. Fiolka, L. Shao, E. H. Rego, M. W. Davidson, and M. G. L. Gustafsson, "Time-lapse two-color
362 3D imaging of live cells with doubled resolution using structured illumination," *Proc. Natl. Acad.*
363 *Sci. U. S. A.* **109**, 5311–5315 (2012).

364 17. A. G. York, S. H. Parekh, D. D. Nogare, R. S. Fischer, K. Temprine, M. Mione, A. B. Chitnis, C.
365 A. Combs, and H. Shroff, "Resolution doubling in live, multicellular organisms via multifocal
366 structured illumination microscopy," *Nat. Methods* **9**, 749–754 (2012).

367 18. M. Ingaramo, A. G. York, P. Wawrzusin, O. Milberg, A. Hong, R. Weigert, H. Shroff, and G. H.
368 Patterson, "Two-photon excitation improves multifocal structured illumination microscopy in
369 thick scattering tissue," *Proc. Natl. Acad. Sci. U. S. A.* **111**, 5254–9 (2014).

370 19. A. G. York, P. Chandris, D. D. Nogare, J. Head, P. Wawrzusin, R. S. Fischer, A. Chitnis, and H.
371 Shroff, "Instant super-resolution imaging in live cells and embryos via analog image processing.,"
372 *Nat. Methods* **10**, 1122–6 (2013).

373 20. M. Schropp and R. Uhl, "Two-dimensional structured illumination microscopy," *J. Microsc.* **256**,
374 23–36 (2014).

375 21. M. Schropp, C. Seebacher, and R. Uhl, "XL-SIM: Extending Superresolution into Deeper
376 Layers," *Photonics* **4**, 33 (2017).

377 22. T. A. Planchon, L. Gao, D. E. Milkie, M. W. Davidson, J. A. Galbraith, G. Catherine, C. G.
378 Galbraith, and E. Betzig, "Rapid three-dimensional isotropic imaging of living cells using Bessel
379 beam plane illumination," *Nat. Methods* **8**, 417–423 (2011).

380 23. P. J. Keller, A. D. Schmidt, A. Santella, K. Khairy, Z. Bao, J. Wittbrodt, and E. H. K. Stelzer,
381 "Fast, high-contrast imaging of animal development with scanned light sheet-based structured-
382 illumination microscopy," *Nat Meth* **7**, 637–642 (2010).

1
2
3
4
5
6
7
8
9
10
11
12
13
14
15
16
17
18
19
20
21
22
23
24
25
26
27
28
29
30
31
32
33
34
35
36
37
38
39
40
41
42
43
44
45
46
47
48
49
50
51
52
53
54
55
56
57
58
59
60
61
62
63
64
65

383 24. L. Gao, L. Shao, C. C. D. Higgins, J. S. J. Poulton, M. Peifer, M. W. Davidson, X. Wu, B.
384 Goldstein, and E. Betzig, "Noninvasive imaging beyond the diffraction limit of 3D dynamics in
385 thickly fluorescent specimens," *Cell* **151**, 1370–1385 (2012).

386 25. B.-C. Chen, W. R. Legant, K. Wang, L. Shao, D. E. Milkie, M. W. Davidson, C. Janetopoulos, X.
387 S. Wu, J. A. Hammer, Z. Liu, B. P. English, Y. Mimori-Kiyosue, D. P. Romero, A. T. Ritter, J.
388 Lippincott-Schwartz, L. Fritz-Laylin, R. D. Mullins, D. M. Mitchell, J. N. Bembenek, A.-C.
389 Reymann, R. Bohme, S. W. Grill, J. T. Wang, G. Seydoux, U. S. Tulu, D. P. Kiehart, and E.
390 Betzig, "Lattice light-sheet microscopy: Imaging molecules to embryos at high spatiotemporal
391 resolution," *Science* **346**, 1257998 (2014).

392 26. D. Li, L. Shao, B.-C. Chen, X. Zhang, M. Zhang, B. Moses, D. E. Milkie, J. R. Beach, J. A.
393 Hammer, M. Pasham, T. Kirchhausen, M. A. Baird, M. W. Davidson, P. Xu, and E. Betzig,
394 "Extended-resolution structured illumination imaging of endocytic and cytoskeletal dynamics,"
395 *Science* **349**, aab3500 (2015).

396 27. S. Dong, P. Nanda, R. Shiradkar, K. Guo, and G. Zheng, "High-resolution fluorescence imaging
397 via pattern-illuminated Fourier ptychography.," *Opt. Express* **22**, 20856–70 (2014).

398 28. F. Orieux, E. Sepulveda, V. Lorient, B. Dubertret, and J.-C. Olivo-Marin, "Bayesian estimation
399 for optimized structured illumination microscopy.," *IEEE Trans. Image Process.* **21**, 601–14
400 (2012).

401 29. T. Lukeš, G. M. G. M. Hagen, P. Křížek, Z. Švindrych, K. Fliegel, M. Klíma, P. Křížek, Z.
402 Švindrych, K. Fliegel, and M. Klíma, "Comparison of image reconstruction methods for
403 structured illumination microscopy," *Proc. SPIE* **9129**, 91293J (2014).

404 30. T. Lukeš, P. Křížek, Z. Švindrych, J. Benda, M. Ovesný, K. Fliegel, M. Klíma, and G. M. Hagen,
405 "Three-dimensional super-resolution structured illumination microscopy with maximum a
406 posteriori probability image estimation," *Opt. Express* **22**, 29805–17 (2014).

407 31. E. Mudry, K. Belkebir, J. Girard, J. Savatier, E. Le Moal, C. Nicoletti, M. Allain, and A.

1
2
3
4
5
6
7
8
9
10
11
12
13
14
15
16
17
18
19
20
21
22
23
24
25
26
27
28
29
30
31
32
33
34
35
36
37
38
39
40
41
42
43
44
45
46
47
48
49
50
51
52
53
54
55
56
57
58
59
60
61
62
63
64
65

408 Sentenac, "Structured illumination microscopy using unknown speckle patterns," *Nat. Photonics*
409 **6**, 312–315 (2012).

410 32. X. Huang, J. Fan, L. Li, H. Liu, R. Wu, Y. Wu, L. Wei, H. Mao, A. Lal, P. Xi, L. Tang, Y. Zhang,
411 Y. Liu, S. Tan, and L. Chen, "Fast, long-term, super-resolution imaging with Hessian structured
412 illumination microscopy," *Nat. Biotechnol.* (2018).

413 33. V. Perez, B. J. Chang, and E. H. K. Stelzer, "Optimal 2D-SIM reconstruction by two filtering
414 steps with Richardson-Lucy deconvolution," *Sci. Rep.* **6**, 37149 (2016).

415 34. K. Chu, P. J. McMillan, Z. J. Smith, J. Yin, J. Atkins, P. Goodwin, S. Wachsmann-Hogiu, and S.
416 Lane, "Image reconstruction for structured-illumination microscopy with low signal level," *Opt.*
417 *Express* **22**, 8687 (2014).

418 35. N. Chakrova, B. Rieger, and S. Stallinga, "Deconvolution methods for structured illumination
419 microscopy," *J. Opt. Soc. Am. A* **33**, B12 (2016).

420 36. P. Křížek, T. Lukeš, M. Ovesný, K. Fliegel, and G. M. Hagen, "SIMToolbox: A MATLAB
421 toolbox for structured illumination fluorescence microscopy," *Bioinformatics* **32**, 318–320 (2015).

422 37. P. Křížek, I. Raška, and G. M. Hagen, "Flexible structured illumination microscope with a
423 programmable illumination array," *Opt. Express* **20**, 24585 (2012).

424 38. G. M. Hagen, W. Caarls, M. Thomas, A. Hill, K. A. Lidke, B. Rieger, C. Fritsch, B. van Geest, T.
425 M. Jovin, and D. J. Arndt-Jovin, "Biological applications of an LCoS-based programmable array
426 microscope," *Proc. SPIE* **64410S**, 1–12 (2007).

427 39. C. A. Werley, M.-P. Chien, and A. E. Cohen, "An ultrawidefield microscope for high-speed
428 fluorescence imaging and targeted optogenetic stimulation," *Biomed. Opt. Express* **8**, 5794
429 (2017).

430 40. D. Dan, M. Lei, B. Yao, W. Wang, M. Winterhalder, A. Zumbusch, Y. Qi, L. Xia, S. Yan, Y.
431 Yang, P. Gao, T. Ye, and W. Zhao, "DMD-based LED-illumination super-resolution and optical
432 sectioning microscopy.," *Sci. Rep.* **3**, 1116 (2013).

1
2
3
4
5
6
7
8
9
10
11
12
13
14
15
16
17
18
19
20
21
22
23
24
25
26
27
28
29
30
31
32
33
34
35
36
37
38
39
40
41
42
43
44
45
46
47
48
49
50
51
52
53
54
55
56
57
58
59
60
61
62
63
64
65

433 41. P. Křížek and G. M. Hagen, "Spatial light modulators in fluorescence microscopy," in
434 *Microscopy: Science, Technology, Applications and Education*, A. Méndez-Vilas, ed., 4th ed.
435 (Formatex, 2010), Vol. 2, pp. 1366–1377.

436 42. G. M. Hagen, W. Caarls, K. A. Lidke, A. H. B. De Vries, C. Fritsch, B. G. Barisas, D. J. Arndt-
437 Jovin, and T. M. Jovin, "Fluorescence recovery after photobleaching and photoconversion in
438 multiple arbitrary regions of interest using a programmable array microscope," *Microsc. Res.*
439 *Tech.* **72**, 431–440 (2009).

440 43. L. Song, H.-W. Lu-Walther, R. Förster, A. Jost, M. Kielhorn, J. Zhou, and R. Heintzmann, "Fast
441 structured illumination microscopy using rolling shutter cameras," *Meas. Sci. Technol.* **27**,
442 055401 (2016).

443 44. Z. Cvačková, M. Mašata, D. Staněk, H. Fidlerová, and I. Raška, "Chromatin position in human
444 HepG2 cells: although being non-random, significantly changed in daughter cells.," *J. Struct.*
445 *Biol.* **165**, 107–17 (2009).

446 45. L. J. Young, F. Ströhl, and C. F. Kaminski, "A Guide to Structured Illumination TIRF
447 Microscopy at High Speed with Multiple Colors," *J. Vis. Exp.* e53988–e53988 (2016).

448 46. R. Förster, H.-W. Lu-Walther, A. Jost, M. Kielhorn, K. Wicker, and R. Heintzmann, "Simple
449 structured illumination microscope setup with high acquisition speed by using a spatial light
450 modulator," *Opt. Express* **22**, 20663–77 (2014).

451 47. H.-W. Lu-Walther, M. Kielhorn, R. Förster, A. Jost, K. Wicker, and R. Heintzmann, "fastSIM: a
452 practical implementation of fast structured illumination microscopy," *Methods Appl. Fluoresc.* **3**,
453 014001 (2015).

454 48. T. C. Schlichenmeyer, M. Wang, K. N. Elfer, and J. Q. Brown, "Video-rate structured
455 illumination microscopy for high-throughput imaging of large tissue areas.," *Biomed. Opt.*
456 *Express* **5**, 366–77 (2014).

457 49. S. R. Kantelhardt, W. Caarls, A. H. B. de Vries, G. M. Hagen, T. M. Jovin, W. Schulz-Schaeffer,

1
2
3
4
5
6
7
8
9
10
11
12
13
14
15
16
17
18
19
20
21
22
23
24
25
26
27
28
29
30
31
32
33
34
35
36
37
38
39
40
41
42
43
44
45
46
47
48
49
50
51
52
53
54
55
56
57
58
59
60
61
62
63
64
65

458 V. Rohde, A. Giese, and D. J. Arndt-Jovin, "Specific visualization of glioma cells in living low-
459 grade tumor tissue," *PLoS One* **5**, 1–11 (2010).

460 50. J. Pospíšil, K. Fliegel, and M. Klíma, "Assessing resolution in live cell structured illumination
461 microscopy," in *Proceedings of SPIE - The International Society for Optical Engineering*, P. Páta
462 and K. Fliegel, eds. (SPIE, 2017), Vol. 10603, p. 39.

463 51. A. K. Agarwal, N. Srinivasan, R. Godbole, S. K. More, S. Budnar, R. P. Gude, and R. D.
464 Kalraiya, "Role of tumor cell surface lysosome-associated membrane protein-1 (LAMP1) and its
465 associated carbohydrates in lung metastasis.," *J. Cancer Res. Clin. Oncol.* **141**, 1563–74 (2015).

466 52. Pospíšil J; Lukeš T; Bendesky J; Fliegel K; Spendier K; Hagen GM (2018): Supporting data for
467 "Imaging tissues and cells beyond the diffraction limit with structured illumination microscopy
468 and Bayesian image reconstruction" GigaScience Database. <http://dx.doi.org/10.5524/100514>

469 53. F. Huang, T. M. P. Hartwich, F. E. Rivera-Molina, Y. Lin, W. C. Duim, J. J. Long, P. D. Uchil, J.
470 R. Myers, M. A. Baird, W. Mothes, M. W. Davidson, D. Toomre, and J. Bewersdorf, "Video-rate
471 nanoscopy using sCMOS camera-specific single-molecule localization algorithms.," *Nat.*
472 *Methods* **10**, 1–9 (2013).

473 54. J. W. Goodman, "Frequency Analysis of Optical Imaging Systems," in *Introduction to Fourier*
474 *Optics*, 2nd ed. (McGraw-Hill Int., 1968), pp. 126–171.

475 55. M. Geissbuehler and T. Lasser, "How to display data by color schemes compatible with red-green
476 color perception deficiencies.," *Opt. Express* **21**, 9862–74 (2013).

477 **FIGURE CAPTIONS**

478 **Figure 1:** Structured illumination microscope setup, which we used with different microscope bodies and
479 cameras. See text and table 2 for details.

480 **Figure 2:** Measurements of the spatial resolution on a sample of fluorescent beads. Cross-sections of the
481 PSF are obtained by averaging measurements over 50 beads along lateral and axial directions.

1
2
3
4
5
6
7
8
9
10
11
12
13
14
15
16
17
18
19
20
21
22
23
24
25
26
27
28
29
30
31
32
33
34
35
36
37
38
39
40
41
42
43
44
45
46
47
48
49
50
51
52
53
54
55
56
57
58
59
60
61
62
63
64
65

Figure 3: Resolution analysis and normalized power spectral density (PSD) measured on a selected image from the data in Fig. 5. The results indicate a circularly-averaged PSD lateral spatial resolution of 294 nm for WF, and 141 nm for MAP-SIM, in approximate agreement with the analysis in Fig. 4(d-f).

Figure 4: Imaging live cells beyond the diffraction limit with MAP-SIM. U2-OS cells expressing LAMP1-GFP were imaged using the LCOS-based SIM system. Subsequent processing using OS-SIM or MAP-SIM methods. (a) WF, (b) OS-SIM, (c) MAP-SIM, (d) FFT of WF, (e) FFT of OS-SIM, (f) FFT of MAP-SIM. The images were individually scaled for presentation. The dotted circular lines indicate the approximate resolution achieved in each image according to analysis of the FFT. The full image sequence is available at http://mmtg.fel.cvut.cz/mapsimlive_suppl/.

Figure 5: Imaging live cells beyond the diffraction limit with SIM. A431 cells labeled with DiI-C16 were imaged using the LCOS-based SIM system. Subsequent processing using SR-SIM or MAP-SIM methods. (a) WF, (c) SR-SIM, (e) MAP-SIM. (b), (d), and (f) each show a zoom-in of the region indicated in (a). (g) shows the SIM illumination pattern in one of the four angles used. (h) shows a FFT of the image in (g). The images were individually scaled for visualization purposes. Each is a maximum intensity projection of 3 Z positions (spacing 400 nm (except for g and h which show a single Z-position)).

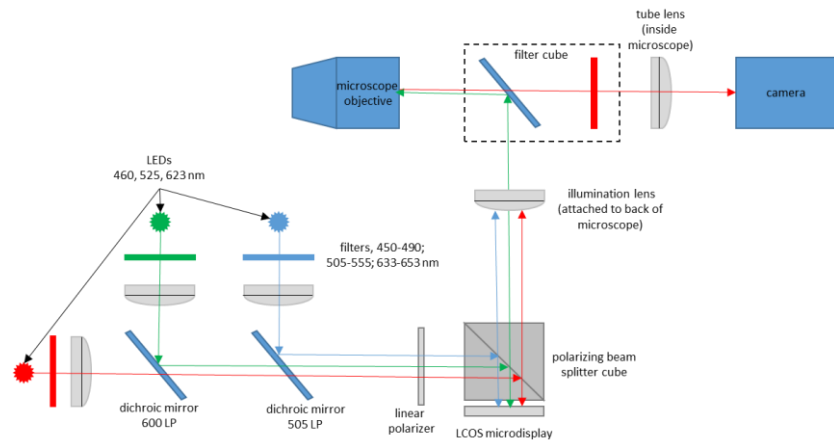
Figure 6: Imaging animal tissues using the LCOS-based SIM system and subsequent processing using OS-SIM or MAP-SIM methods. Seminiferous tubule of the rabbit stained with hematoxylin and eosin. (a) WF, (c) OS-SIM, (e) MAP-SIM. (b), (d), and (f) each show a zoom-in of the region indicated in (a). (g) shows the SIM illumination pattern in one of the four angles used. (h) MAP-SIM depth-coded using the lookup table isolum [55]. The images were individually scaled for visualization purposes. Each is a maximum intensity projection of 31 Z-positions (spacing 300 nm (except for (a, b, g) which show 1 Z-position)).

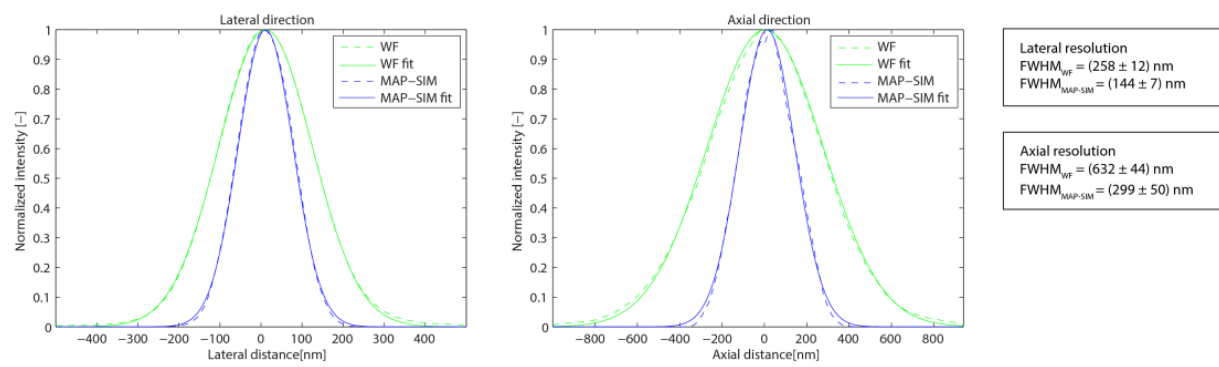
Figure 7: SIM imaging of fixed HEP-G2 cells expressing Dendra2-H4 (nucleus) and labeled with Atto-532 phalloidin. (a) WF, (c) SR-SIM, (e) MAP-SIM. (b), (d), and (f) each show a zoom-in of the region

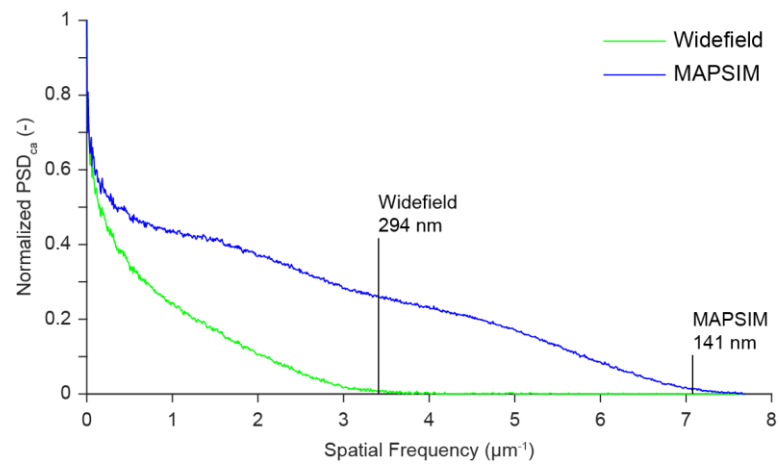
1
2
3
4
5
6
7
8
9
10
11
12
13
14
15
16
17
18
19
20
21
22
23
24
25
26
27
28
29
30
31
32
33
34
35
36
37
38
39
40
41
42
43
44
45
46
47
48
49
50
51
52
53
54
55
56
57
58
59
60
61
62
63
64
65

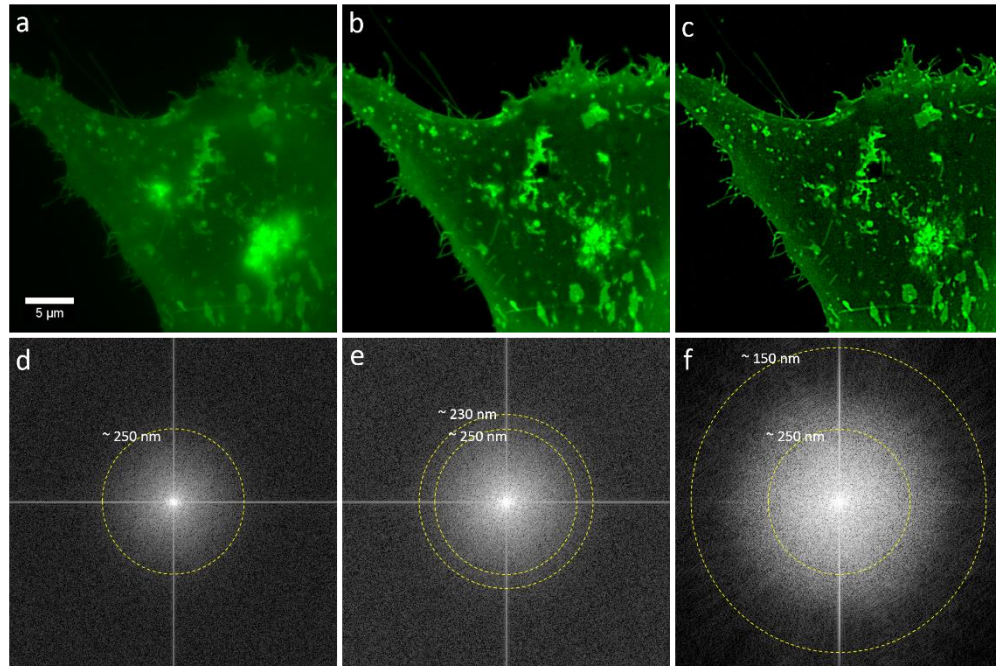
507 indicated in (a). (g) shows the SIM illumination pattern in one of the four angles used. (h) shows a FFT
508 of the image in (g). The images were individually scaled for visualization purposes. Each is a maximum
509 intensity projection of 22 Z-positions (spacing 200 nm (except for a, b, g and h which show 1 Z-
510 position).

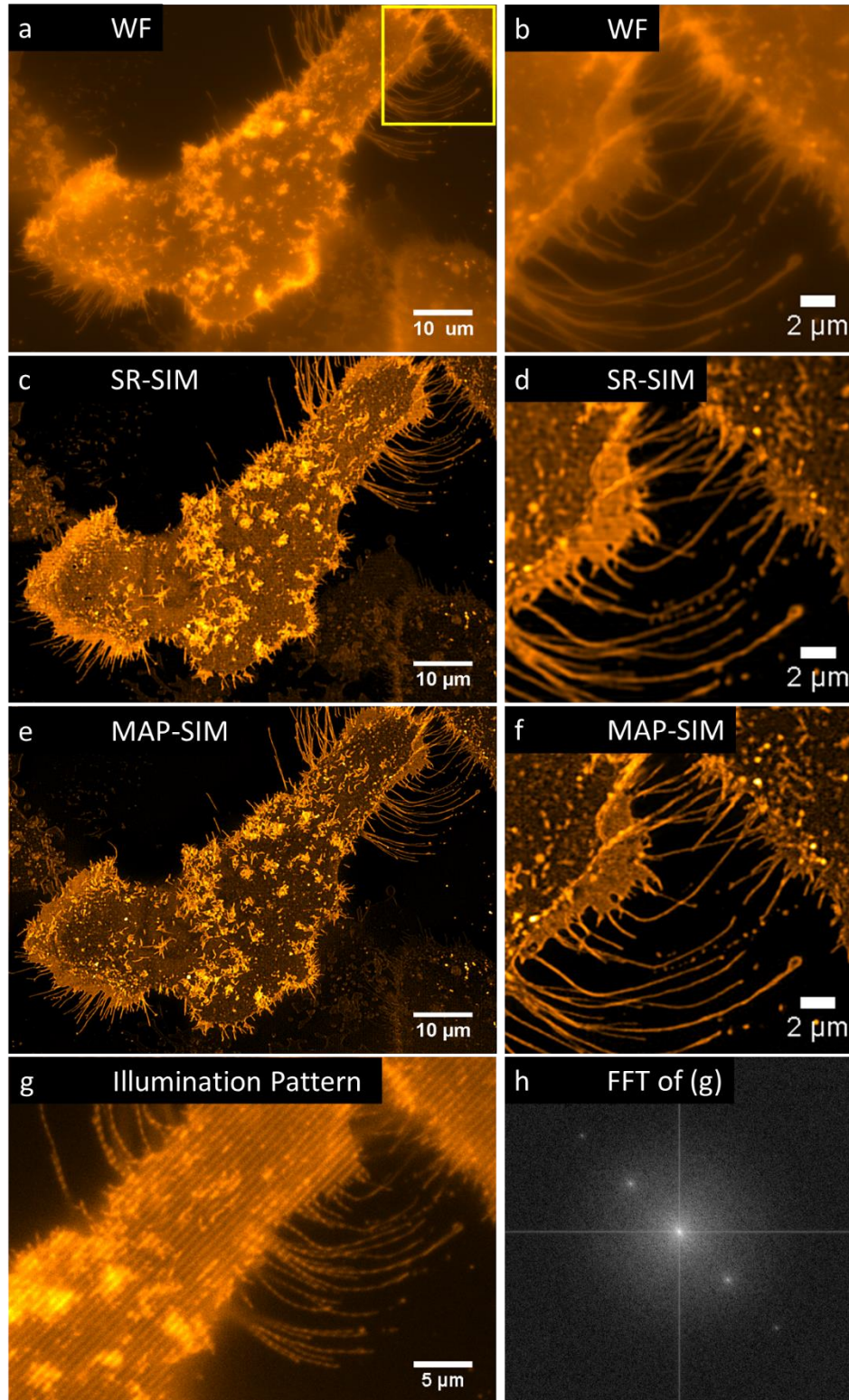
511 **Figure 8:** 2D SIM imaging of fixed BPAE cells labeled with Alexa 488-phalloidin (actin) and
512 mitotracker CMXRos (mitochondria). (a) WF, (b) MAPSIM.

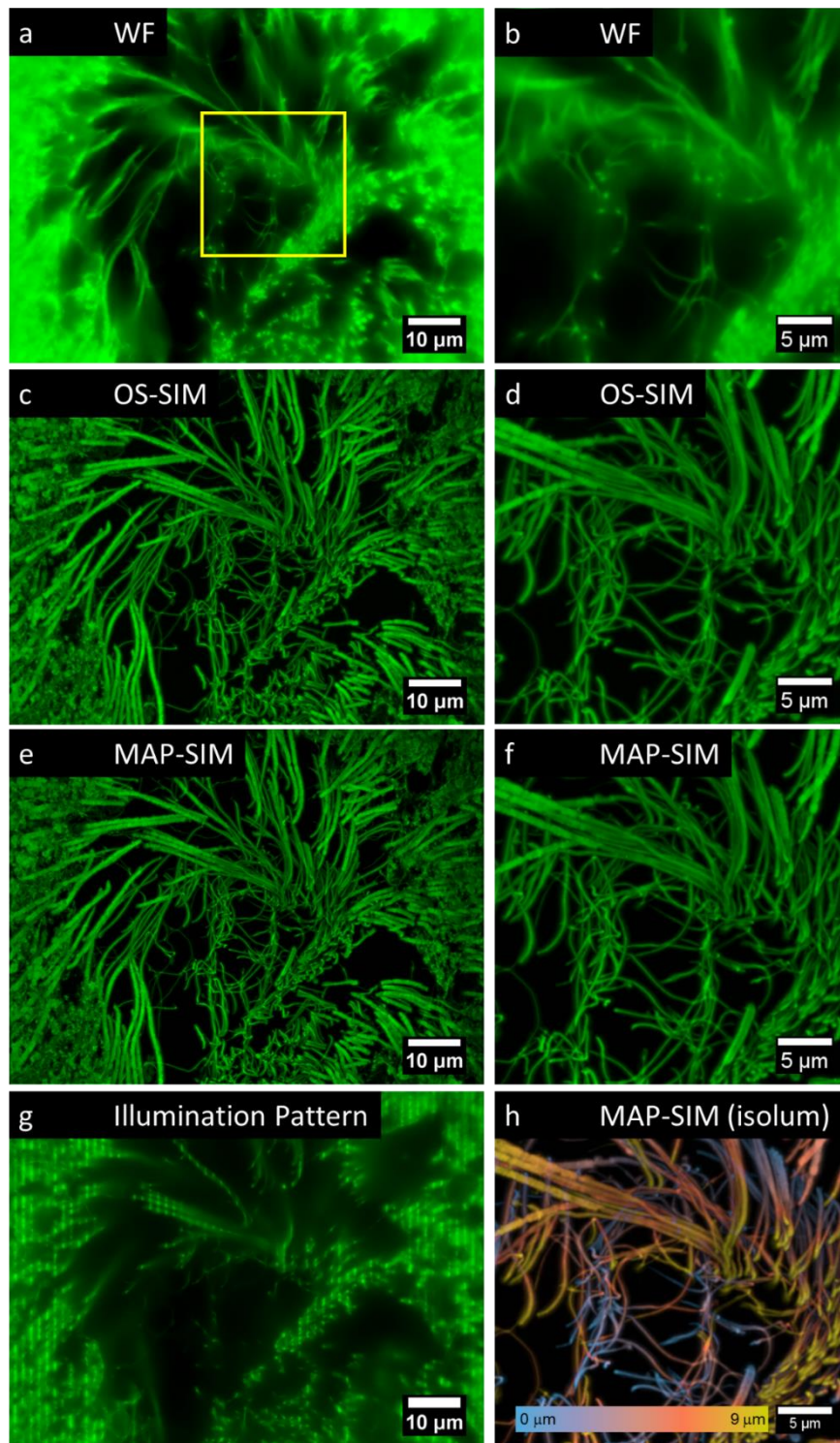


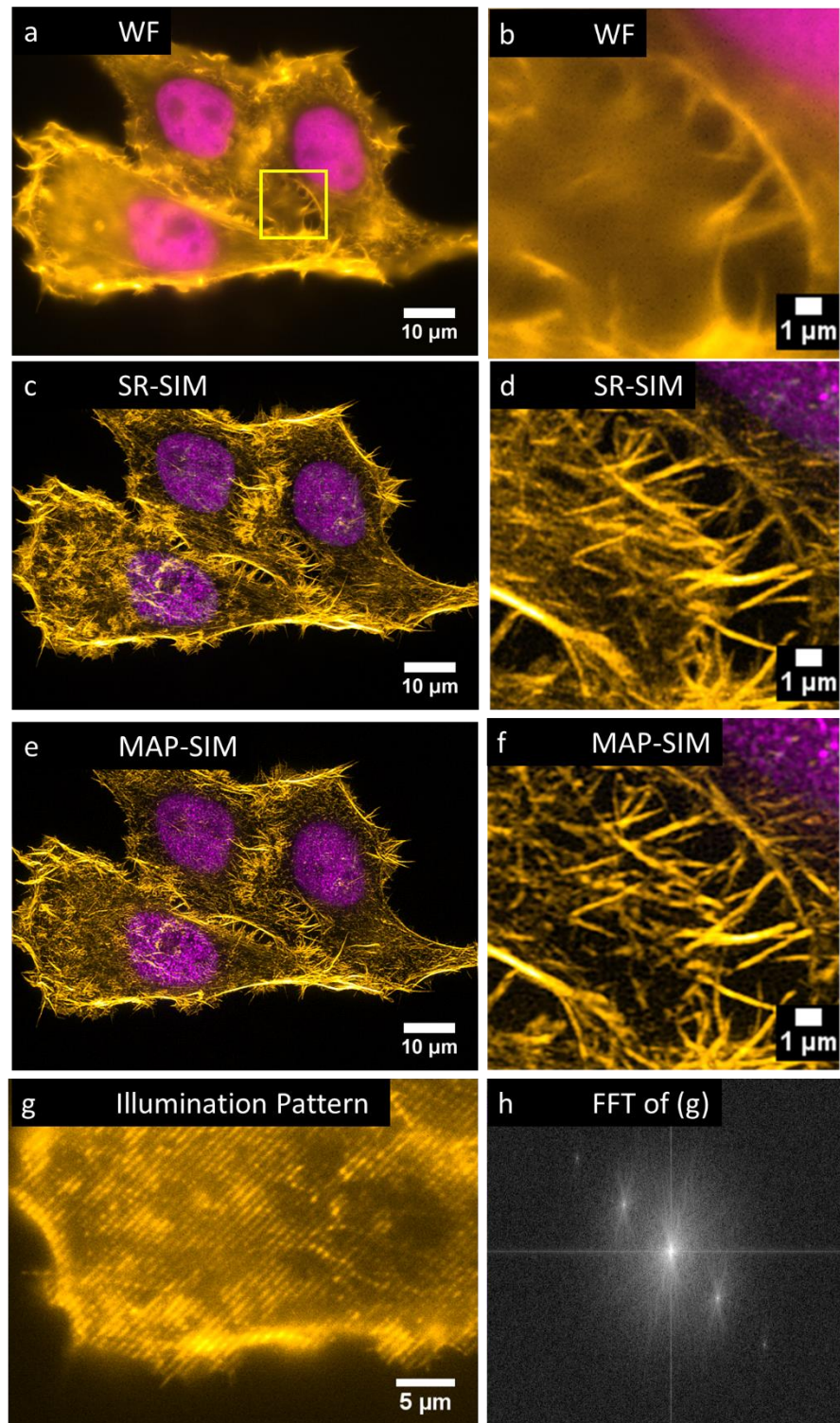


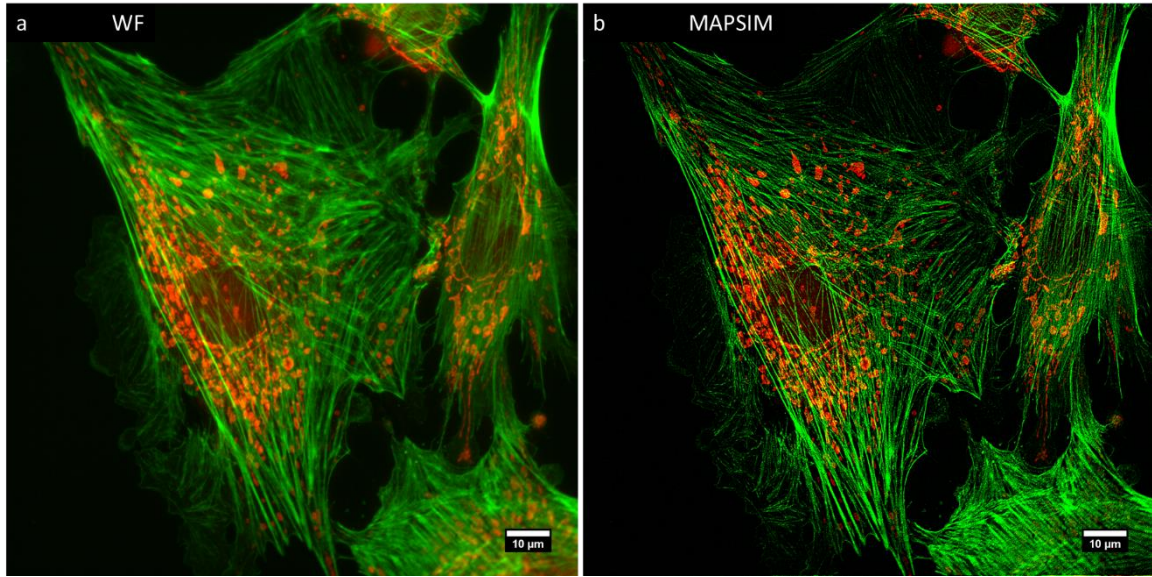














[Click here to access/download](#)

Supplementary Material

Hagen-SIM Supplementary-resubmit.docx





University of Colorado
Colorado Springs

Dr. Guy M. Hagen

Biofrontiers

1420 Austin Bluffs Pkwy.

Colorado Springs, CO 80918

Tel. 719-255-3692

ghagen@uccs.edu

Dear Editor:

We would like to resubmit our manuscript entitled “Imaging tissues and cells beyond the diffraction limit with structured illumination microscopy and Bayesian image reconstruction” for consideration in *GigaScience* as a data note.

We would like to thank the referees for their very positive reviews of the paper. Reviewer 1 had a minor point of concern:

“One minor point the authors may want to address is the difference between coherent interference illumination and the incoherent pattern illumination employed in the manuscript. It seems that interference illumination can generate a sin pattern with highest contrast at cutoff frequency while incoherent pattern illumination may suffer from the gradually cutoff of the incoherent OTF.”

We thank the reviewer for this comment. The reviewer is correct about this, and we have written some comments and added a new reference in the discussion which should clear up this matter. The modified paragraph now reads:

“There are several other advantages to the use incoherent illumination in SIM, including removing the need for a pupil plane mask to block unwanted diffraction orders. Also, incoherent imaging of a microdisplay for pattern formation means that the pattern spatial frequency in the sample plane does not depend on the wavelength of the light which is used. On the other hand, in incoherent illumination SIM such as we used here, the contrast of the illumination pattern decreases with increasing spatial frequency according to the incoherent optical transfer function [53]. In coherent illumination SIM [8,9,11], the coherent optical transfer function applies [53], and so the pattern contrast does not decrease with increasing spatial frequency. This means that coherent illumination SIM can more efficiently mix high resolution information from outside the frequency limit into the detection passband of the microscope, thereby potentially achieving better resolution than what we achieved in this work. We achieved a lateral resolution enhancement factor of ~ 1.8 (Fig. 2), whereas a factor of 2.0 is expected for coherent illumination SIM.”

In addition to this, we have fixed a few typographical errors.

We hope that the paper will now be acceptable for publication.

Sincerely,

A handwritten signature in blue ink that reads 'Guy Hagen'.

Guy M. Hagen